Analyst

ROYAL SOCIETY OF CHEMISTRY

PAPER

View Article Online
View Journal

Cite this: DOI: 10.1039/c9an02122a

Ratiometric fluorescent sensing of the parallel G-quadruplex produced by PS2.M: implications for K^+ detection†

Prashant S. Deore and Richard A. Manderville *

Received 23rd October 2019,
Accepted 20th December 2019

DOI: 10.1039/c9an02122a

rsc.li/analyst

Fluorescent ligands that selectively bind to a specific G-quadruplex (GQ) topology (antiparallel, hybrid or parallel) are highly sought after for aptasensor development and nanodevice construction. The coumarin–benzothiazole hybrid (BnBtC) is an internal charge transfer (ICT) ratiometric fluorescent probe, which displays two well-resolved emission bands at ~450 nm for the coumarin component and ~650 nm for the ICT band. The red ICT emission of BnBtC displays turn-on responses to protic solvent polarity and upon binding GQ structures, especially those produced by the hemin binding aptamer (PS2.M). In the present work, BnBtC was found to exhibit enhanced ICT emission upon binding the parallel GQ topology of PS2.M that is selectively produced in the presence of K^+. This ability to discriminate K^+ from other cationic metal ions through a turn-on ratiometric fluorescent response demonstrates the potential utility of the BnBtC probe for biosensor applications.

1. Introduction

G-Quadruplexes (GQs) are secondary nucleic acid structures produced by G-rich oligonucleotides that contain stacked G-tetrads connected *via* loop residues.[1–3] They are stabilized by Hoogsteen hydrogen-bonding, G-tetrad stacking and cation coordination within the central cavity of the G-tetrad. They can also exhibit structural diversity and produce parallel, antiparallel or hybrid topologies, which are illustrated by the GQ structures afforded by the human telomeric DNA repeat sequence.[4,5]

The GQ structure is a common recognition element for aptasensor development with diagnostic applications.[6] Here, the GQ-folding aptamer is typically incorporated into a DNA nanodevice that undergoes controlled conformational changes to activate a sensing mechanism.[3,7] Examples include GQ-single-strand,[8] GQ-duplex[9] or a GQ-GQ nanodevice[10] that takes advantage of the intrinsic structural polymorphism of GQ structures. Optical/fluorescent ligands that selectively bind to a specific GQ topology[11,12] and display a readout signal upon target binding are useful for construction of DNA nanodevices.[13–15] Such devices have previously been utilized by our laboratory for aptasensor-based detection of thrombin[16–18] and the food toxin, ochratoxin A.[10,19]

Typical fluorescent probes used as signal readout molecules for GQ structures (*i.e.* Thiazole Orange (TO),[20] protoporphyrin IX (PPIX),[21] Crystal Violet (CV),[22] and Thioflavin T (ThT)),[23] act as single emission sensors with quenched fluorescence in H_2O that lights-up upon GQ binding. However, sensors with two or more emission wavelengths can serve as ratiometric probes and possess critical advantages over single emission sensors for microenvironment monitoring and quantifying levels of target analytes with high selectivity and sensitivity.[24,25] In this regard, we recently reported the ability of the coumarin–hemicyanine hybrid probe (BnBtC, Scheme 1) to ratiometrically discriminate biopolymer targets with superior binding selectivity towards hemin binding aptamer (PS2.M) over other examined GQ-forming nucleic acid targets.[26] BnBtC is an internal charge transfer (ICT) ratiometric fluorescent probe with two well-resolved emission bands at ~450 nm for the coumarin component and ~650 nm for the ICT band. PS2.M binding by BnBtC causes preferential light-up of the red-shifted ICT band at 650 nm. However, because PS2.M exhibits structural polymorphism depending on the nature of the metal ion,[27,28] we were curious to further explore the interaction between BnBtC and PS2.M and determine whether the probe would exhibit ratiometric emission sensitivity toward a specific GQ structure fueled by the addition of metal ions. We now report that BnBtC displays preferential ICT emission for the parallel GQ of PS2.M, permitting ratiometric K^+ detection in the presence of other cationic metal ions, particularly Na^+ with the dye responding to changes in GQ topology within a GQ-GQ nanodevice (Scheme 1). While numerous GQ-based K^+ sensors have

Departments of Chemistry & Toxicology, University of Guelph, Guelph, Ontario, N1G 2W1, Canada. E-mail: rmanderv@uoguelph.ca

†Electronic supplementary information (ESI) available. See DOI: 10.1039/c9an02122a

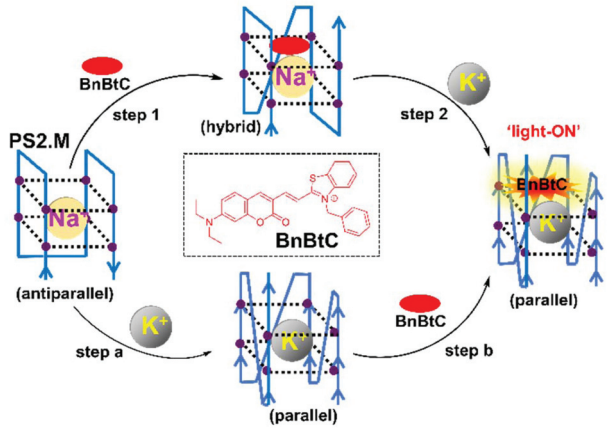

Scheme 1 A representation for the GQ → GQ conformational switch with turn-on response of BnBtC probe to the parallel GQ structure produced by PS2.M in the presence of K^+. Step 2 involves K^+-mediated conformational switch which is recognized by the light-up response of BnBtC probe. Inset: Structure of coumarin–hemicyanine hybrid (BnBtC) probe. The sequence of native PS2.M aptamer is 5′-GTGGGTAGGGCGGGTTGG-3′.

been designed,[28–36] examples of ratiometric K^+ detection have been limited to the use of dual end-labelled GQ-folding oligonucleotides either containing two terminal fluorophores that undergo fluorescence resonance energy transfer (FRET)[32] or two pyrene chromophores to generate pyrene excimer emission[33] upon formation of the GQ mediated by K^+ ion addition. To the best of our knowledge the present work outlines the first example of a label-free GQ-based ratiometric K^+ sensor derived from a single GQ-specific dye.

2. Experimental

2.1 Materials and methods

The HPLC purified native 18-mer G-rich DNA (PS2.M) was purchased from Sigma-Aldrich Ltd (Oakville, ON), suspended in Milli-Q water and quantified using nanodrop. UV absorbance at 256 nm, with ε = 177 400 L mol^{-1} cm^{-1}. The sample of BnBtC was available in our laboratory and was synthesized as described.[26] The 2 mM stock solution was prepared by dissolving it in a spectroscopic grade DMSO prior to dilution with aqueous buffer solution for spectrophotometric measurements in which the DMSO content was assumed negligible. Water used for buffers or spectroscopic solutions was obtained from a filtration system (18.2 MΩ). 200 mM tris-acetate buffer was prepared fresh as a 10× stock buffer solution by dissolving tris base in milli-Q water and pH was adjusted to 6.7 using aqueous acetic acid. 100 mM EDTA solution was prepared as a 10× stock solution in milli-Q water. All metal ion solutions including Na^+ and K^+ were prepared as 20 mM stock solutions in milli-Q water. The sampling for real-life experiment was done by acquiring the water samples from drinking water fountain as mineral water, regular tap water and water from the speed river, Guelph, ON, Canada. The samples were used as acquired for analysis. All the UV-Vis, fluorescence and CD studies were performed in a 20 mM tris-acetate buffer at ambient temperature (~25 °C) except for CD spectra which were acquired at 15 °C. The data shown is averaged from minimum of three replicates of each experiment which were performed independently.

2.2 Fluorescence measurements

Fluorescence spectra were acquired on the Edinburgh Instrument Spectrofluorometer FS5 in quartz cells (108.002F-QS) with a path length of 10 × 2 mm. Whereas, other fluorescence responses were acquired on the Spectramax i3 instrument using 384 well plate as an average of 25-point scans. The fluorescence measurements were performed using the BnBtc probe with the excitation and emission wavelengths were set at 367/550 and 645 nm, respectively. Also, the DNA and dye in the sample buffer were used in 1 : 5 molar ratio with PS2.M at 1 μM and BnBtC at 5 μM concentration. The K^+ binding study was performed in the 20 mM tris-acetate buffer containing 100 mM NaCl. Binding constant (K_d value) was obtained from the binding isotherm plot of the fraction of aptamer folded *versus* K^+ concentration, and it was generated using sigma plot 11.0 software with one site saturation – simple ligand binding model. The limit of detection (LoD) and quantification (LoQ) were based on the standard deviation of the response and the slope of calibration curve and were determined by the equations; LoD = $3.3\sigma/s$ and LoQ = $10\sigma/s$, where, σ = standard error of estimate obtained by standard deviation of the *y*-intercept of the regression line sy/x; and s = slope of calibration curve.[37] The selectivity experiment for K^+ against other metal ions was carried out in 20 mM tris-acetate buffer containing 10 mM EDTA. EDTA was added to diminish the effect of certain heavy metal ions such as Pb^{2+} by forming metal–EDTA complex, these metal ions can interfere with the DNA secondary structures. The probe performance in real-life water samples, such as mineral water, tap water and water collected from the speed river that were spiked with the certain amount of K^+ and analyzed using Spectramax i3 instrument. All these measurements were performed in an independent triplicate using the Spectramax i3 instrument using 384 well plate and averaged values were reported.

2.3 UV-Visible measurements and thermal denaturation studies

Acquisition of all UV-Vis spectra and melting temperature (T_m) measurements were performed on a Cary 300-Bio UV-vis spectrophotometer. Absorbance spectra displayed in Fig. 1b was acquired for BnBtC (15 μM) with or without PS2.M (3 μM) in presence of 100 mM of Na^+/K^+ in tris-acetate buffer. Melting temperatures (T_m) for GQ of PS2.M (3 μM) in Na^+/K^+ (100 mM) independently in presence of BnBtC (15 μM) in tris-acetate buffer. The temperature was ramped between 10–90 °C with an increment of 0.5 °C min^{-1} and monitored at 295 nm as a function of temperature. T_m values were established by determining the first derivative of the DNA melting curves using Varian thermal software as an average of four ramps.

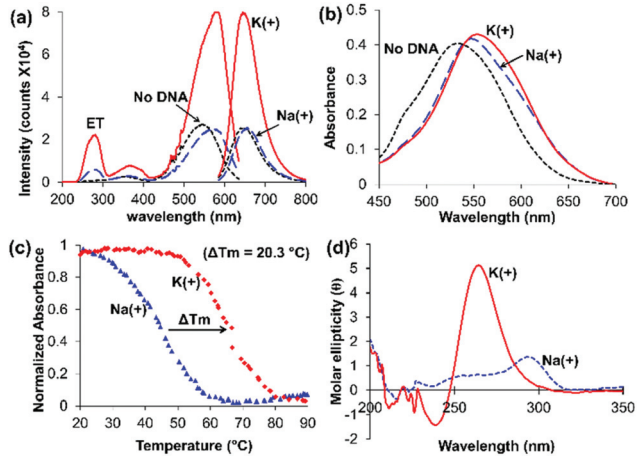

Fig. 1 (a) Fluorescence excitation and emission spectra of BnBtC (5 μM) in presence of Na^+/K^+ (dotted black traces) and PS2.M–BnBtC complex (1 : 5 μM) separately in presence of Na^+ (100 mM, dashed blue traces) and K^+ (100 mM, solid red traces) solutions. (b) UV-Vis spectra of BnBtC (15 μM) in presence of Na^+/K^+ (dotted black traces) and PS2.M–BnBtC complex (3 : 15 μM) separately in presence of Na^+ (100 mM, dashed blue traces) and K^+ (100 mM, solid red traces) solutions. (c) The UV-melting curves for the G-quadruplex of PS2.M (3 μM) induced by Na^+ (100 mM, blue trace) and K^+ (100 mM, red trace) in the presence of BnBtC dye (15 μM) which were measured at 295 nm with temperature ramped at 0.5 °C min^{-1}. (d) CD spectra of PS2.M (5 μM) induced by Na^+ (100 mM) and K^+ (100 mM), respectively in the presence of BnBtC (25 μM) probe. All measurements were performed in 20 mM tris-acetate buffer (pH = 6.7) at ambient temperature.

2.4 CD measurements

CD spectra were obtained on a Jasco J-815 CD spectrophotometer equipped with a thermally controlled 1 × 6 multicell block. It was performed in quartz cells (110-QS) with a light path of 1 mm and monitored between 200–400 nm at a bandwidth of 1 nm and scanning speed of 100 nm min^{-1} at 15 °C. Samples of PS2.M (3 and 5 μM) were prepared in tris-acetate buffer containing no metal ions or Na^+/K^+ in 100 mM concentration and with or without BnBtC (25 μM, 5 equivalents to DNA). The CD spectra were recorded immediately after manual mixing of the samples.

3. Results and discussion

3.1 GQ structure-specific binding by BnBtC

The binding of BnBtC to GQ structures produced by PS2.M in the presence of Na^+ and K^+ was investigated using UV-Visible, fluorescence and circular dichroism (CD) spectroscopies (Fig. 1 and Fig. S1, ESI†). The fluorescence of BnBtC (PS2.M : BnBtC, 1 : 5 μM) displayed ~3-fold turn-on of emission intensity induced by binding to the GQ structure of PS2.M in the presence of K^+ (100 mM KCl, Fig. 1a). In contrast, little change in fluorescence intensity was observed for BnBtC binding to PS2.M in the presence of 100 mM NaCl. The excitation spectra of BnBtC with PS2.M displayed a prominent energy transfer (ET) band at ~256 nm, which is indicative of dye stacking interactions with the G-tetrad.[38] A significantly greater ET band was noted in presence of K^+ (~31-fold increase compared to the free dye, Fig. 1a and Fig. S1a†) compared to Na^+ (~8-fold increase, Fig. 1a and Fig. S1b†), suggesting superior stacking interactions with the GQ produced by K^+ addition. The ratiometric emission response of the PS2.M–BnBtC system was recorded with excitation at 367 displayed a 13 nm red-shift in absorbance wavelength in 100 mM Na^+ solution (λ_{Abs} = 546 nm), whereas in 100 mM K^+ solution nm and displayed turn-on fluorescence at 650 nm in K^+ solution, while virtually no response was observed in the presence or absence of Na^+ (Fig. S2†). As shown in Fig. 1b, the absorbance traces of the PS2.M–BnBtC system (3 μM : 15 μM) displayed a 20 nm red-shifted absorbance (λ_{Abs} = 553 nm) when compared to that of the free dye in solution (λ_{Abs} = 533 nm).

Native PS2.M displays a GQ UV-thermal melting temperature (T_m) of 46 °C and 58 °C in the presence of Na^+ and K^+, respectively,[39] exhibiting a notable stabilization (ΔT_m = 12 °C) for the GQ structure produced by K^+ over Na^+. BnBtC binding (5 equivalents) to PS2.M afforded a T_m of 44.6 °C (ΔT_m = −1.6 °C) in the presence of Na^+ (blue trace, Fig. 1c) and 64.9 °C (ΔT_m = 6.9 °C) in the presence of K^+ (red trace, Fig. 1c). Thus, BnBtC preferentially increased the stability of the GQ produced by K^+ compared to Na^+ with ΔT_m = 20.3 °C. Overall, these experiments provided evidence for preferential binding of the BnBtC probe for the GQ topology of PS2.M produced in the presence of K^+.

Insight into the secondary GQ structures produced by PS2.M in Na^+ and K^+ solutions was provided by measuring CD profiles in the corresponding metal ion solutions (Fig. 1d). The oligonucleotide produces an antiparallel GQ fold in the presence of Na^+, displaying positive peaks at 295 and 250 nm, and negative peaks at 265 and 237 nm (Fig. S3a†). However, the antiparallel fold transformed into the hybrid topology upon addition of BnBtC (up to 5 equivalents) as evidenced by loss of the negative peak at 265 nm (blue trace, Fig. 1d, see changes in Fig. S3a†). In the presence of K^+, PS2.M folds into a parallel topology with a strong positive peak at 265 nm that was ~4-fold more intense than the positive peak of the hybrid fold induced by Na^+ (Fig. 1d) Addition of BnBtC had little impact on the parallel GQ structure produced in K^+ solution (Fig. S3b†). These results clearly indicated the presence of three distinct GQ topologies of PS2.M with the fluorescence of the BnBtC probe preferentially responding to the K^+-stabilized parallel GQ structure (Fig. 1a).

3.2 PS2.M–BnBtC as a K^+ sensor

Given the selectivity displayed by BnBtC upon binding the parallel GQ produced by PS2.M in K^+ solution (Fig. 1), its utility for K^+ detection was explored in more detail by performing fluorescence emission titrations with selective excitation at 367 nm (Fig. 2a). A dose-dependent increase in fluorescence emission intensity at 650 nm for K^+ titration (0 → 200 mM) was observed in 20 mM tris-acetate buffer (pH = 6.7) containing 100 mM of NaCl. Increased ET at ~256 nm was also observed (Fig. S4†). The binding isotherm was plotted (Fig. 2a,

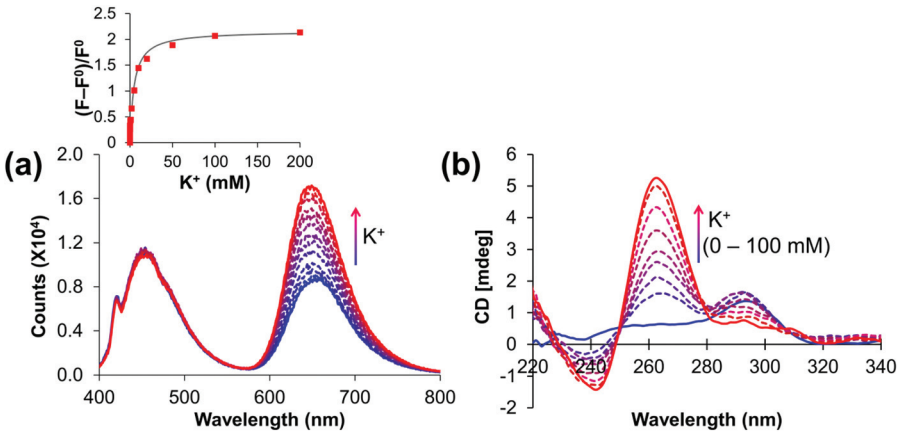

Fig. 2 (a) Ratiometric fluorescence titration of PS2.M–BnBtC (1 : 5 μM, λ_{ex} = 367 nm) and (b) CD spectral titration of PS2.M–BnBtC (3 : 15 μM) with increasing concentration of K^+ (0 → 200 mM, blue to red traces) at 25 and 15 °C, respectively. Inset: Fluorescence responses of PS2.M–BnBtC to increasing concentration of K^+ at 25 °C. Where, F^0 and F are the fluorescence intensities in the absence and varying K^+ concentration, respectively. Dissociation constant, K_d = 4.8 ± 1.0 mM was calculated using sigma plot software with one site saturation – simple ligand binding model. All titrations were performed in 20 mM tris-acetate buffer (pH = 6.7) containing 100 mM NaCl.

inset) for K^+ binding to PS2.M–BnBtC system and an apparent dissociation constant K_d = 4.8 ± 1.0 mM was determined. The analytical validation of the presented K^+ probe was performed by obtaining its limit of detection, LoD = 39 μg mL^{-1} (~1 mM) and limit of quantification, LoQ = 118 μg mL^{-1} (~3 mM) values with R^2 = 0.98 (Fig. S5†). These values are comparable to other label-free platforms presented for K^+ detection using single emission sensors (LoD = 1 mM,[29] and 0.5 mM (ref. 28)). Alternative GQ-based platforms for K^+ detection include colorimetric peroxidase-like DNAzymes[34,35] and dual-labeled oligonucleotides[32,33,36] that boast ultrasensitive LoD values in the low μM-regime. However, the colorimetric signal from the DNAzyme system can be slow to develop for K^+ sensing (~1.5 h),[35] while dual-labeled oligonucleotides can be challenging to synthesize. Furthermore, the concentration of K^+ ion in household drinking water and biological matrices (human serum) are in the mM-regime, making the simple label-free platforms highly practical.

The results were further evidenced from the CD spectral titration of K^+ (0 → 100 mM) into the PS2.M–BnBtC (3 : 15 μM) solution containing 100 mM of Na^+ (Fig. 2b). The loss of intensity at 295 nm with increasing amplitudes at 265 nm (positive) and 240 nm (negative) were a clear indication of conformational switch from hybrid to parallel topology mediated by K^+ additions. The ability of the PS2.M–BnBtC (1 : 5 μM) system to distinguish K^+ from other potential metal ion interferences was also determined (Fig. 3). For these experiments EDTA was added to the buffer solution to trap certain heavy metal ions such as Hg^{2+} and Pb^{2+}, which are known to induce structural changes in DNA.[28,29,40] Under these specific conditions, the

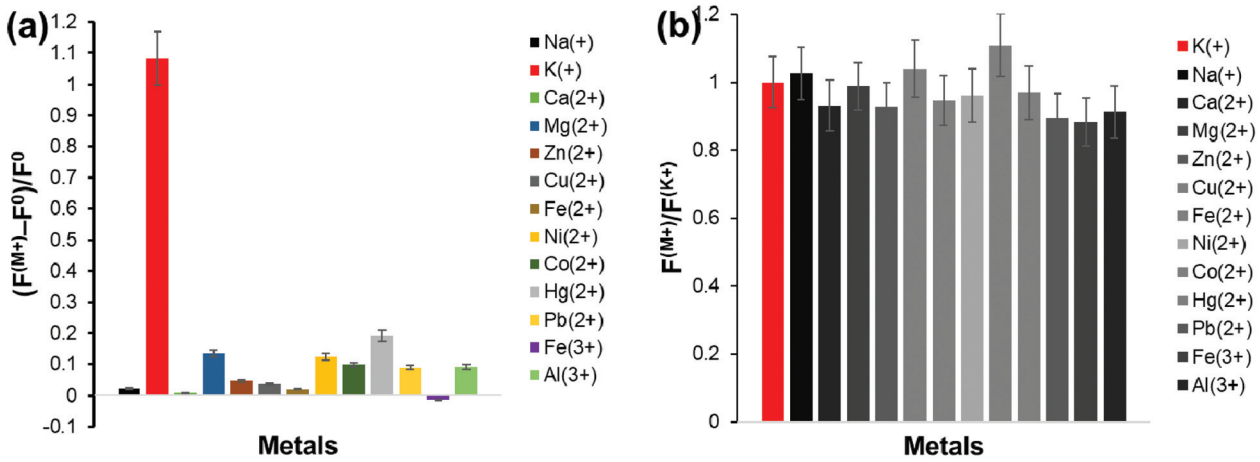

Fig. 3 Selectivity of PS2.M–BnBtC to K^+ detection. Fluorescence responses for (a) presence of individual metal ion (2 mM), and (b) coexistence of the other metal ions (2 mM) with K^+ (2 mM). Spectra were recorded in 20 mM of tris-acetate buffer (pH = 6.7) containing 5 μM of BnBtC, 1 μM of PS2.M and 10 mM of EDTA at ambient temperature and reported values were averaged from three independent measurements. Fluorescence intensities F^0, $F^{(M+)}$ and $F^{(K+)}$ are the intensities obtained in the absence of any metal ion, presence of the metal ions and presence of the K^+, respectively.

parallel GQ-dye platform displayed excellent selectivity for K^+ detection (Fig. 3a).

Moreover, the K^+ selectivity was further demonstrated in a competitive assay, in which the BnBtC probe displayed a consistent ratiometric fluorescence response for K^+ in the presence of other metal ions (Fig. 3b). The PS2.M–BnBtC-based K^+ detection method was further verified by recovery experiments in complex matrices (Table S1†). Three water samples (mineral, tap and river) were spiked with varying K^+ concentrations (1.0 and 2.0 mM) and the average recovery of K^+ was determined as 106, 101.5 and 99.3% for the three samples, respectively. The results suggest that the parallel GQ PS2.M–BnBtC platform may potentially be useful for K^+ determination in real samples.

3.3 Logic gate construction

Applicability of the probe is often investigated by converting chemically encoded information into fluorescence signals.[18,41] In this regard, a logic device containing 'AND' logic functions was envisioned based on the present PS2.M–BnBtC platform for K^+ detection. The two inputs were PS2.M and K^+, respectively and fluorescence response was read at the fluorescence output of 645 nm. Based on Fig. 4a, the threshold fluorescence intensity at 645 nm was set at 2.5×10^4 counts. The intensity higher than the threshold value was assigned as "1", and lower intensity was assigned as "0" portraying the "signal-ON" and "signal-OFF" responses, respectively. The truth table depicted in Fig. 4b was drawn for various possible combinations of these two chemical inputs. While, the fluorescence response at 645 nm output is read as 1 (signal-ON) or 0 (signal-OFF), as depicted in Fig. 4c, which was based on threshold fluorescence intensity. Output values from the truth table suggested AND logic functions for the PS2.M–BnBtC platform and logic gate was constructed as shown in Fig. 4d.

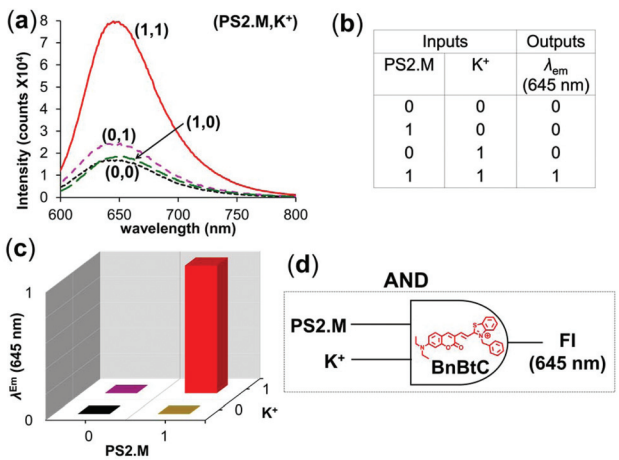

Inputs		Outputs
PS2.M	K^+	λ_{em} (645 nm)
0	0	0
1	0	0
0	1	0
1	1	1

Fig. 4 (a) Fluorescence emission spectra of BnBtC at different chemical inputs, namely no-input (0,0), PS2.M (1,0), K^+ (0,1) and PS2.M + K^+ (1,1). Based on these results, fluorescence threshold intensity of 2.5×10^4 counts was assigned at 645 nm. (b) The truth table for combinatorial logic circuit, where '0' = 'off' and '1' = 'on' signals. (c) Fluorescence emission results of BnBtC probe at different inputs (0/1) according to the truth table. Intensity above and below the threshold value (2.5×10^4 counts) are assigned as '1' and '0', respectively. (d) 'AND" logic gate has been constructed based on results obtained from the figures a, b and c described previously.

4. Conclusions

In summary, the ratiometric coumarin–hemicyanine hybrid (BnBtC) probe selectively targets the parallel GQ topology produced by the hemin binding DNA aptamer (PS2.M) in the presence of K^+. Parallel GQ binding by BnBtC causes preferential increase in the ICT emission at ~650 nm. In contrast, the emission of BnBtC exhibits only minor changes compared to free dye emission when binding Na^+-PS2.M, which favors an antiparallel topology that is converted into the hybrid upon BnBtC binding. This observation permitted the construction of a metal fueled GQ-GQ nanodevice with the BnBtC probe responding to parallel GQ formation (Scheme 1). The PS2.M–BnBtC platform was then investigated as a ratiometric sensor for K^+ and was found to display an LoD = ~1 mM with excellent selectivity for K^+ in the presence of other potential metal ion interferences. Current efforts in our laboratory are focused on the site-specific insertion of ratiometric dye types into DNA aptamers to probe changes in the microenvironment of the probe upon target binding and to generate new ratiometric aptasensors for diagnostic applications.

Conflicts of interest

There are no conflicts to declare.

Acknowledgements

This project was funded by the Natural Sciences and Engineering Research Council of Canada, Discovery Grant to RAM [NSERC-Discovery, 2018-04621].

References

1 J. Choi and T. Majima, *Chem. Soc. Rev.*, 2011, **40**, 5893–5909.
2 M. L. Bochman, K. Paeschke and V. A. Zakian, *Nat. Rev. Genet.*, 2012, **13**, 770–780.
3 J. L. Mergny and D. Sen, *Chem. Rev.*, 2019, **119**, 6290–6325.
4 I. Prisian, J. Lah and G. Vesnaver, *J. Am. Chem. Soc.*, 2008, **130**, 14161–14169.
5 M. Sproviero, K. L. Fadock, A. A. Witham and R. A. Manderville, *ACS Chem. Biol.*, 2015, **10**, 1311–1318.
6 Y. Du and S. Dong, *Anal. Chem.*, 2017, **89**, 189–215.
7 D. Li, S. P. Song and C. H. Fan, *Acc. Chem. Res.*, 2010, **43**, 631–641.

8 D. Monchaud, P. Yang, L. Lacroix, M. P. Teulade-Fichou and J. L. Mergny, *Angew. Chem., Int. Ed.*, 2008, **47**, 4858–4861.
9 P. Alberti and J. L. Mergny, *Proc. Natl. Acad. Sci. U. S. A.*, 2003, **100**, 1569–1573.
10 P. S. Deore, M. D. Gray, A. J. Chung and R. A. Manderville, *J. Am. Chem. Soc.*, 2019, **141**, 14288–14297.
11 B. R. Vummidi, J. Alzeer and N. W. Luedtke, *ChemBioChem*, 2013, **14**, 540–558.
12 S. Asamitsu, T. Bando and H. Sugiyama, *Chem. – Eur. J.*, 2019, **25**, 417–430.
13 Y. Du, B. Li and E. Wang, *Acc. Chem. Res.*, 2013, **46**, 203–213.
14 Q. Chen, J. Zuo, J. Chen, P. Tong, X. Mo, L. Zhang and J. Li, *Biosens. Bioelectron.*, 2015, **72**, 326–331.
15 D. M. Engelhard, J. Nowack and G. H. Clever, *Angew. Chem., Int. Ed.*, 2017, **56**, 11640–11644.
16 M. Sproviero and R. A. Manderville, *Chem. Commun.*, 2014, **50**, 3097–3099.
17 K. L. Fadock, R. A. Manderville, P. Sharma and S. D. Wetmore, *Org. Biomol. Chem.*, 2016, **14**, 4409–4419.
18 P. S. Deore, D. V. Soldatov and R. A. Manderville, *Sci. Rep.*, 2018, **8**, 16874.
19 K. L. Fadock and R. A. Manderville, *ACS Omega*, 2017, **2**, 4955–4963.
20 Y. P. Xing, C. Liu, X. H. Zhou and H. C. Shi, *Sci. Rep.*, 2015, **5**, 8125.
21 G. Ma, Z. Yu, W. Zhou, Y. Li, L. Fan and X. Li, *J. Phys. Chem. B*, 2019, **123**, 5405–5411.
22 S. Wang, J. Zhao, S. Lu, J. Sun and X. Yang, *Chem. Commun.*, 2019, **55**, 1911–1914.
23 A. C. Bhasikuttan and J. Mohanty, *Chem. Commun.*, 2015, **51**, 7581–7597.
24 M. H. Lee, J. S. Kim and J. L. Sessler, *Chem. Soc. Rev.*, 2015, **44**, 4185–4191.
25 M. A. Haidekker and E. A. Theodorakis, *J. Mater. Chem. C*, 2016, **4**, 2707–2718.
26 P. S. Deore, D. S. Coman and R. A. Manderville, *Chem. Commun.*, 2019, **55**, 3540–3543.
27 T. Li, E. Wang and S. Dong, *J. Am. Chem. Soc.*, 2009, **131**, 15082–15083.
28 T. Li, E. Wang and S. Dong, *Anal. Chem.*, 2010, **82**, 7576–7580.
29 L. Liu, Y. Shao, J. Peng, C. Huang, H. Liu and L. Zhang, *Anal. Chem.*, 2014, **86**, 1622–1631.
30 H. Cheng, X. Qiu, X. Zhao, W. Meng, D. Zuo and H. Wei, *Anal. Chem.*, 2016, **88**, 2937–2943.
31 X. Sun, Q. Li, J. Xiang, L. Wang, X. Zhang, L. Lan, S. Xu, F. Yang and Y. Tang, *Analyst*, 2017, **142**, 3352–3355.
32 H. Ueyama, M. Takagi and S. Takenaka, *J. Am. Chem. Soc.*, 2002, **124**, 14286–14287.
33 S. Nagatoishi, T. Nojima, B. Juskowiak and S. Takenaka, *Angew. Chem., Int. Ed.*, 2005, **44**, 5067–5070.
34 T. Li, E. Wang and S. Dong, *Chem. Commun.*, 2009, 580–582.
35 X. Yang, T. Li, B. Li and E. Wang, *Analyst*, 2010, **135**, 71–75.
36 A. Verdian-Doghaei, M. R. Housaindokht and Kh. Abnous, *Anal. Biochem.*, 2014, **466**, 72–75.
37 A. Shrivastava and V. B. Gupta, *Chron. Young Sci.*, 2011, **2**, 21–25.
38 A. Dumas and N. W. Luedtke, *Nucleic Acids Res.*, 2011, **39**, 6825–6834.
39 Y. Liu, J. Ren, Y. Qin, J. Li, J. Liu and E. Wang, *Chem. Commun.*, 2012, **48**, 802–804.
40 L. Berti and G. A. Burley, *Nat. Nanotechnol.*, 2008, **3**, 81–87.
41 Y. Guo, L. Zhou, L. Xu, X. Zhou, J. Hu and R. Pei, *Sci. Rep.*, 2014, **4**, 7315.

